Continuous solar-driven gasification of oil palm agricultural bio waste for high-quality syngas production

Srirat Chuayboon, Stéphane Abanades

Continuous solar-driven gasification of oil palm agricultural bio waste for high-quality syngas production

Srirat Chuayboon[a,b], Stéphane Abanades[a,*]

[a] Processes, Materials and Solar Energy Laboratory, PROMES-CNRS, 7 Rue du Four Solaire, 66120 Font-Romeu, France

[b] Department of Mechanical Engineering, King Mongkut's Institute of Technology Ladkrabang, Prince of Chumphon Campus, Chumphon 86160, Thailand

**Corresponding author*: Tel +33 (0)4 68 30 77 30

E-mail address: stephane.abanades@promes.cnrs.fr

Abstract

Empty fruit bunch (EFB) from oil palm is a solid agricultural bio-waste obtained from the edible oil process. Continuous solar-driven gasification of EFB offers a bright carbon-neutral avenue to convert both EFB bio-waste and renewable solar energy into sustainable and clean syngas. High-temperature concentrated solar heat is used to provide the reaction enthalpy, and therefore biomass waste feedstock is entirely dedicated to produce hydrogen and carbon monoxide (syngas). Solar energy is stored as a high-quality syngas and can be easily transported as a convertible and dispatchable chemical form. In this study, the performance of continuous steam gasification of EFB, fully powered by concentrated solar heat, was experimentally investigated in a solar gasification reactor. Experiments were carried out with continuous EFB biomass injection to evaluate the influence of temperature (1100-1300 °C) and biomass feeding rate (0.5-1.8 g/min). As a result, syngas yields and reactor performance were substantially enhanced by rising the EFB feeding rate and gasification temperature. An optimal EFB biomass feeding rate enabling maximum gasification performance was found to be 1.4 g/min at 1300 °C and 1.0 g/min at 1200 °C. Carbon conversion approaching 97%, energy upgrade factor of 1.38, and solar-to-fuel energy conversion efficiency up to 20% were demonstrated. Finally, the maximum syngas yield was found to be 81.1 mmol/$g_{dry\ biomass}$ at 1300 °C (with H_2 and CO as the main constituents), closely approaching the maximum theoretical expected value reached at thermodynamic equilibrium. Combining concentrated solar energy and biomass waste gasification was shown to be a promising and sustainable pathway toward waste valorization into carbon-neutral solar fuels.

Keywords: solar fuel, biomass, bio-waste, EFB bioresource, gasification, solar reactor.

1. Introduction

Fossil fuel depletion and climate change associated with global warming are of major concern (Thomas & Prasad, 2003). Because of the increased fossil fuel consumption and environmental concerns, developing clean renewable energy for green fuel and power production is needed. Renewable energies include solar energy, biomass, wind, and geothermal (Beck & Martinot, 2004). Among them, solar energy and biomass are of particular interest. Indeed, solar energy is by far the most plentiful, accessible, reliable, and clean renewable energy. Once concentrated, solar energy can be used as an external heat source at high-temperature, depending on the magnitude of the solar concentration (Moriarty

& Honnery, 2019). On the other hand, biomass is widely available as bio-wastes from various processing industries, municipal solid waste sources, agricultural production, forestry, and plantations (palm, sugar, rice, etc.) (Bonechi et al., 2017). Importantly, Thailand has great potential in both renewable solar energy (Chimres & Wongwises, 2016) and agricultural solid biomass supply, particularly bio-waste from oil palm plantations (Prasertsan & Prasertsan, 1996). The oil palm is an agro-industrial commodity that is used to produce cooking oil and fuels (biodiesel). The residues of cultivated palm oil plantations are plentiful, and consist of tree branches (31%), fiber material (18%), fruit shell (10%), fronds and trunks (38%), and palm kernels (4%) (Prasertsan & Sajjakulnukit, 2006; Shuit et al., 2009).

The production of syngas from oil palm biomass using thermochemical conversion processes such as biomass gasification is energetically favorable thanks to the attractive potential availability of oil palm biomass in Thailand, its chemical properties (high content in hydrogen and lignocellulosic components), and its high calorific value (Hossain et al., 2016; Prasertsan & Sajjakulnukit, 2006). The gasification technology is conventional and is originally based on auto-thermal reaction conditions. It is used for converting solid carbonaceous materials such as biomass, organic and/or inorganic wastes, to synthesis gas (H_2 and CO mixture). Importantly, syngas is regarded as an energy carrier for multi-applications such as H_2 and bio-liquid fuels production (Ashokkumar et al., 2022; Materazzi & Taylor, 2019), as well as a fuel for the direct combustion process. Conventional gasification has been applied for converting agricultural biomass to biofuel (Pohjakallio et al., 2020) for several decades. However, it faces several major drawbacks. For example, a significant amount of biomass feedstock (up to 40% in total) is internally burnt with oxygen in air for driving the endothermic gasification reaction. As a result, this portion of biomass feedstock is unavoidably wasted (Kabli et al., 2022) instead of being converted to syngas.

Additionally, syngas products are contaminated by combustion products such as CO_2, tar, and solid carbon (You et al., 2017), which downgrades syngas quality.

Alternatively, solar biomass gasification offers a promising avenue to integrate two renewable energies (both solid biomass and solar energy) in a single process (Bellouard et al., 2017; Boujjat et al., 2019a; Chuayboon et al., 2018b; Chuayboon et al., 2019). With this concept, concentrated solar energy provides an external heat source to drive the gasification reaction (Ling et al., 2022). Therefore, the gasification reaction can take place without any partial combustion (Lichty et al., 2010), instead biomass feedstock is fully dedicated to syngas production. With this approach, syngas production from solar biomass gasification can be considered as carbon-neutral (Abanades et al., 2021; Chuayboon & Abanades, 2020). An experimental parametric study of continuous beech wood biomass gasification with steam was performed in a solar reactor up to 1300 ºC (Chuayboon et al. (2018b). The influence of biomass feedstock type, particle size, and feeding rate on thermochemical performances of a continuous solar gasification reactor was investigated (Chuayboon et al., 2018a; Chuayboon et al., 2019). Increasing the feeding rate promoted the solar-to-fuel energy efficiency beyond 25%. Parametric optimization of solar-driven steam gasification of EFB via central composite design was also achieved (Al-Muraisy et al., 2022). Moreover, hybrid solar gasification is an attractive approach to overcome the variability of solar energy and operate continuously (Boujjat et al., 2020a; Rodat et al., 2020). Boujjat et al. (2019a) investigated hybrid solar/autothermal steam gasification of wood biomass and performed numerical simulations of reactive gas-particle flow in a solar gasification reactor. The gasification temperature can be controlled by O_2 injection during sun-lacking periods for continuous biomass gasification. In addition, dynamic simulation and control of solar biomass gasification established the strategies for maximum syngas yield production over day and night based on real solar irradiation data (Boujjat et al., 2021; Boujjat et al., 2020c).

Nipattummakul et al. (2011) studied conventional steam gasification of oil palm residual bunches using a semi-batch reactor in the temperature range of 600-1000 °C. A parametric study considering the influence of temperature and steam-to-solid fuel ratio on syngas composition was emphasized, and a gasification temperature of less than 700 °C was not recommended. Moreover, pyrolysis of oil palm wastes with Ni, γ-Al_2O_3, Fe_2O_3 and La/Al_2O_3 catalysts at 400-900 °C was studied to promote the cracking of hydrocarbons and tar in the vapor phase and the hydrogen yield (Li et al., 2009; Yang et al., 2006). In addition, oil palm kernel shells were utilized as solid feedstock in a conventional downdraft air gasification process to produce syngas (Dechapanya et al., 2020; Tsai, 2019). For example, Basha et al. (2020) studied air co-gasification of oil palm kernel shell and polystyrene using an electrically-heated gasifier and reported the issues associated with tar yield and polystyrene mixture. Apart from oil palm wastes, rice husk (Sarasuk & Sajjakulnukit, 2011) and sugar cane (Jahromi et al., 2021) wastes were intensively studied via conventional gasification process. However, the ash content in the dry rice husk is high (up to 25 wt%) which caused ash accumulation problems during the process (Steven et al., 2021). In addition, Vargas-Mira et al. (2019) reported different biomass gasification methods (direct or indirect gasification, and supercritical water gasification) and purification technologies to improve the operating process for hydrogen production from oil palm EFB. Chu et al. (2022) performed a pilot-scale municipal solid waste gasification driven by partial feedstock combustion. Recently, chemical-looping gasification was proposed to enhance syngas quality by avoiding direct fuel-air mixing, although yielding CO_2 from the fuel reactor (Roshan Kumar et al., 2022). Solar-assisted biomass chemical-looping gasification with solar heat absorbed by oxygen carrier particles was also proposed (Chuayboon et al., 2018c; Sun and Aziz, 2022).

From the previous studies, most works applied conventional gasification under autothermal conditions to convert oil palm biomass, which caused biomass losses and low-quality syngas (Lapuerta et al., 2008; Mohammed et al., 2012; Omar et al., 2011). Some studies tried to increase the syngas yield by adding catalysts while others focused on solar gasification of woody biomass (Boujjat et al., 2020b; Boujjat et al., 2019b; Boujjat et al., 2020c). However, solar gasification of agricultural bio-wastes performed under real solar radiation was not considered before.

Therefore, the present study aims to experimentally investigate the continuous gasification of oil palm waste residues using concentrated solar energy as the external heat source to drive gasification reactions. Empty fruit bunch (EFB) from oil palm was selected due to its high availability and suitable properties (Mohammed et al., 2012; Omar et al., 2011). A directly-irradiated particle-fed solar reactor was utilized and operated with a solar tracking system under concentrated sunlight irradiation. The solar reactor and methodology used in this study were previously developed for the gasification of woody biomass (Chuayboon et al., 2018a,b). In the current work, the solar process was applied to the conversion of waste feedstocks to demonstrate that such a process is flexible and can accommodate various kinds of feedstock aiming at the valorization of wastes for the synthesis of valuable fuels.

The ideal stoichiometric reaction of solar steam gasification of EFB (with an empirical formula as $C_7H_{12}O_5$) is written as:

$$C_7H_{12}O_5 + 2H_2O + \text{solar heat} \rightarrow 7CO + 8H_2 \quad (1)$$

In the continuous solar gasification process, biomass feeding rate plays a significant role on gasification performance. An increase in the biomass feeding rate should enhance syngas production capacity. However, an excessively high feeding rate may result in incomplete biomass gasification and accumulation in the reactor cavity receiver, causing pyrolytic gas release (Chuayboon et al., 2019). The biomass feeding rate must be optimized to maximize the syngas yield and solar reactor performance. A trade-off in biomass feeding rate at any specified temperature is needed for maximizing the gasification performance during continuous solar gasification. Minimizing the heat losses is also required to improve energy upgrade factor and solar-to-fuel energy conversion efficiency (Chuayboon et al., 2018a). The effect of EFB biomass feeding rate on continuous gasification performance at different temperatures was thus evaluated thoroughly. The high-temperature solar reactor was successfully operated continuously under different waste feeding rates to determine different relevant performance metrics encompassing the syngas production rate, carbon conversion, energy upgrade factor, and solar-to-fuel energy conversion efficiency. The beneficial effect of increasing the temperature or the waste feeding rate on syngas yields, production rates, energy upgrade factors and efficiencies was highlighted. Such a process combining solar energy utilization for the conversion and upgrading of waste feedstocks to high-value solar fuels was investigated here for the first time. With the integration of these two renewable energy sources (solar energy and EFB bio-waste), solar-driven thermochemical gasification may become a novel sustainable and green approach for the industrial conversion of a waste feedstock to valuable synthetic fuel.

2. Experimental setup and methods

2.1 EFB preparation and characterization

In this study, the high-temperature solar gasification of biomass waste from the palm oil industry for thermochemical syngas production is considered. **Table 1** shows the proximate and ultimate analyses of EFB obtained from the edible oil process in Chumphon province, Thailand. It was cut into small particles with a grinder machine with a size distribution between 1-2 mm.

2.2 Experimental setup

The lab-scale experimental facility for the continuous solar gasification of EFB is presented in **Fig. 1**. The reactor is designed for being coupled with real concentrated sunlight. The solar concentrating system consists of an automatic sun-tracking heliostat and a 2-m diameter parabolic solar concentrator (thermal power up to 1.5 kW at the focal point with a solar flux density as high as 12,000 kW/m^2 for Direct Normal Irradiation DNI of 1 kW/m^2). As shown in **Fig. 1a**, the solar reactor is directly irradiated and continuously operated. It is mainly composed of a cavity receiver, water-cooled reactor shell, hemispherical transparent window, and biomass feeding delivery system. The cavity receiver is made of alumina and wrapped by an insulation layer. The alumina cap with a 17-mm aperture is placed on top of the cavity receiver to close it. Reactor temperatures (T_1-T_3) are measured by B-type thermocouples and are compared with a pyrometer measurement ($T_{pyrometer}$). Reactor pressures are measured by pressure transducers (P_1-P_3). Ar and steam flow rates are regulated by thermal mass flow controllers. More details of the solar reactor were provided in previous work (Chuayboon et al., 2018c).

As illustrated in **Fig. 1b**, direct sunlight is reflected by an automatic sun-tracking heliostat towards a solar concentrator. Subsequently, concentrated solar radiations enter the reactor cavity directly via the aperture through a transparent glass window in the downward direction. The reactor is heated gradually under argon flow (Ar). Solar power input is controlled by an automatic shutter installed between the automatic-tracking heliostat and the parabolic dish concentrator. In each experiment, EFB (20 g for each run) was injected along with a constant Ar flow rate of 0.5 NL/min by the particle delivery system into the reactor cavity receiver. In the meantime, steam was injected with a constant Ar carrier gas of 0.2 NL/min via the cavity receiver bottom in the upward direction. The steam/EFB molar ratio was controlled and kept constant at 2.2 at any EFB biomass feeding rate (slight steam excess of around 10% with respect to the stoichiometric steam/EFB biomass molar ratio). Such a slight steam excess is necessary to favor EFB-to-syngas conversion and alleviate pyrolytic smoke formation at low gasification temperatures such as 1100 °C or below (Chuayboon et al., 2019). A protective Ar flow rate of 2.0 NL/min was also injected through two stainless steel tubes to protect the transparent window. The steam gasification reaction of EFB took place under continuous operation. Syngas exited the reactor via the gas products outlet port, and it was then cleaned by the gas filtering unit with a water scrubber and microfilter (pore diameter of 0.1 µm) to remove entrained char particles and unconverted water prior to gas analysis. The concentration of each species in evolved syngas was then measured continuously by an online gas analyzer (GAS 3180P+) and compared with a gas chromatograph (micro-GC, Varian CP4900). All the measured data were recorded by an automatic data collector.

From the known total inert Ar flow rate and the measured species mole fractions (y_i), the production rate of each gas species (F_i) was calculated: $F_i = F_{Ar}.y_i/y_{Ar}$ (presented in the unit of NL/min). The syngas yield was then computed by integrating the gas production rates over operating time, and it is presented in the unit of mmol/$g_{dry\ biomass}$ (millimole per gram of dry EFB biomass). The solar reactor performances were then determined.

The global mass balance according to **Eq. 2** is the ratio of net output (syngas, solid products, and unconverted water) to net input (EFB biomass and water), which indicates how well the mass between input and output is closed.

$$\text{Global mass balance} = \frac{m_{syngas} + m_{solid\ products+water}}{m_{biomass} + m_{oxidant}} \quad (2)$$

where m_i represents the mass of species i (kg).

The carbon conversion (X_C, **Eq. 3**) is the ratio of the carbon contained in the syngas to that contained in the biomass feedstock:

$$X_C = \frac{\int_0^t F_{CO}(t)dt + \int_0^t F_{CO_2}(t)dt + \int_0^t F_{CH_4}(t)dt + \int_0^t 2F_{C_2H_m}(t)dt}{\int_0^t 7F_{C_7H_{12}O_5}(t)dt} \quad (3)$$

where F_i represents the molar flow rate of species i (mol/s).

The energy upgrade factor (U, **Eq. 4**) is the ratio of the energy content of the syngas to that of the EFB biomass feedstock:

$$U = \frac{(LHV_{syngas} \cdot \dot{m}_{syngas})}{(LHV_{feedstock} \cdot \dot{m}_{feedstock})} \quad (4)$$

where LHV_{syngas} and $LHV_{feedstock}$ are the lower heating values of syngas products and biomass feedstock (J/kg), $\dot{m}_{syngas}$ and $\dot{m}_{feedstock}$ are the mass flow rates (kg/s).

The solar-to-fuel energy conversion efficiency ($\eta_{solar-to-fuel}$, **Eq. 5**) is the ratio of the energy content of the syngas to the total energy input (including both the solar power input and the energy content of the EFB biomass feedstock):

$$\eta_{solar-to-fuel} = \frac{(LHV_{syngas} \cdot \dot{m}_{syngas})}{\dot{Q}_{solar} + (LHV_{feedstock} \cdot \dot{m}_{feedstock})} \quad (5)$$

where $\dot{Q}_{solar}$ is the solar power input (W).

3. Results and discussion

3.1 Representative solar experiment of continuous steam gasification of EFB

Waste gasification was experimentally studied in a high-temperature solar reactor under real solar irradiation conditions, with emphasis on the effect of waste feeding rate and temperature on syngas yield and reactor efficiencies. **Fig. 2** shows a representative solar experiment of continuous steam gasification of EFB. The syngas production rates (H_2, CO, CO_2, CH_4, and C_2H_m) and reactor temperature (represented as T_1 measured inside the cavity at the center) were plotted as a function of time. In this test, EFB biomass particles (20 g) were fed at a EFB biomass feeding rate ($\dot{m}_{EFB}$) of 1.0 g/min under a constant steam/EFB molar ratio of 2.2 (slight steam excess) at a temperature (T_1) of 1300 °C. As soon as EFB fell into the reactor cavity receiver, the gasification reaction took place immediately thanks to the high gasification temperature. Syngas flows of H_2, CO, CO_2, and CH_4 reached a peak and then fluctuated slightly around a nominal value due to injection instability from the biomass screw feeder, caused by the low density of EFB and irregular shape and size of fed particles. Overall, a high-quality and energy-rich syngas was produced in a continuous mode (syngas energy content up to 350.3 kJ). H_2 and CO peak production rates exceeded 1.3 and 0.9 NL/min respectively, and their average values were found to be 0.97 NL/min for H_2 and 0.72 NL/min for CO. Extremely low CO_2, CH_4, and C_2H_m production rates were measured thanks to the high gasification temperature. The syngas production rates obtained from the online gas analyzer (solid lines) were in good agreement with those measured by gas chromatography (GC) (dots), thereby confirming results reliability. During the on-sun experiment, the DNI was high and stable at around 1000 W/m² (1 Sun). Note that the yearly average solar radiation resource at the experiment location (Odeillo, France) is favorable for solar processing (above ~1,600 kWh/m²) thanks to the high solar potential in the south of France. The temperature (T_1) was thus stable at 1300 °C throughout the test. The process exhibited remarkable syngas yield and reactor performance. Syngas compounds yields were 39.9 (H_2), 29.2 (CO), 4.2 (CO_2), 2.1 (CH_4), and 0.7 (C_2H_m) mmol/$g_{dry\ biomass}$, resulting in an average H_2/CO ratio of 1.4 over the experiment duration. During this test, EFB biomass conversion into syngas up to 91.3% and global mass balance up to 95% were achieved. The energy upgrade factor (U) and solar-to-fuel energy conversion efficiency ($\eta_{solar-to-fuel}$) exceeded 1.2 and 19% respectively, thereby demonstrating both a significant upgrade of the calorific content of the feedstock and an efficient solar energy storage into syngas.

The endothermic EFB waste gasification reaction was thus fully driven by concentrated sunlight as a high-temperature heat source. This proof-of-concept experiment pointed out a significant progress in the development of innovative solar gasification reactors with operating temperatures up to 1300 ºC and demonstrated the process feasibility and reliability under real solar irradiation conditions.

3.2 Global mass balance

Global mass balance, represented by the ratio of products mass output to reactants mass input, is shown in **Fig. 3**. Syngas products and steam input were quantified by integrating their flow rates with time while unconverted H_2O and char were quantified by weighing the outlet components before and after each experiment. **Fig. 3a** shows a representative global mass balance at 1.4 g/min of EFB biomass feeding rate and 1300 °C. As a result, products mass output (25.31 g) was almost equal to reactants mass input (26.47 g), thereby yielding a 96% global mass balance. Note that a small amount of remaining ash and unconverted char was not quantified and not considered in the global mass balance calculation, which explained its values slightly below 100%. **Fig. 3b** shows the global mass balance as a function of $\dot{m}_{EFB}$ at 1100, 1200, and 1300 °C. As expected, the mass balance globally increased significantly with increasing temperature and was maximum at 1300 °C.

The influence of $\dot{m}_{EFB}$ on the global mass balance was also observed as it tended to increase, reach a peak, and decrease with increasing biomass feeding rate. The effects of temperature and $\dot{m}_{EFB}$ on syngas yield are discussed more in detail in the next section.

3.3 Syngas yield

Fig. 4 shows syngas yields consisting of H_2 (**Fig. 4a**), CO (**Fig. 4b**), CO_2 (**Fig. 4c**), CH_4 (**Fig. 4d**), C_2H_m (**Fig. 4e**), and total syngas yield (**Fig. 4f**), plotted as a function of $\dot{m}_{EFB}$ at 1100 °C, 1200 °C, and 1300 °C. At each temperature, $\dot{m}_{EFB}$ was increased until reaching the maximum value of syngas yield. Therefore, the range of $\dot{m}_{EFB}$ at each temperature was not the same. As a result, with an increase in $\dot{m}_{EFB}$, H_2, CO, CO_2, CH_4, C_2H_m rose considerably regardless of the temperature (**Fig. 4**), showing a beneficial influence of $\dot{m}_{EFB}$ on syngas yield. H_2 (**Fig. 4a**) increased drastically when increasing both $\dot{m}_{EFB}$ and temperature. At 1300 °C, H_2 yield reached a peak of 42.3 mmol/$g_{dry\ biomass}$ at 1.4 g/min and levelled off at 1.8 g/min, indicating an optimal $\dot{m}_{EFB}$. At 1200 °C, H_2 yield reached a peak of 36.1 mmol/$g_{dry\ biomass}$ at 1.0 g/min and then dropped to 33.5 mmol/$g_{dry\ biomass}$ at 1.8 g/min, indicating an optimal $\dot{m}_{EFB}$ around 1.0 g/min. However, at 1000 °C, H_2 yield evolution remained increasing with $\dot{m}_{EFB}$, and an optimal $\dot{m}_{EFB}$ was not reached. This is due to slow gasification kinetics at this temperature, which caused a difficult control of the gasification process, and a limitation of the maximum allowed value of $\dot{m}_{EFB}$. According to **Fig. 4b**, the trend in the CO yield was similar with H_2 as it increased with increasing $\dot{m}_{EFB}$, reached a peak, and then decreased. The peak of CO yield was found at 1.4 g/min (30.8 mmol/$g_{dry\ biomass}$) at 1300 °C, against 1.0 g/min at 1200 °C (25.6 mmol/$g_{dry\ biomass}$) and 1100 °C (21.5 mmol/$g_{dry\ biomass}$).

Fig. 4c, **Fig. 4d**, and **Fig. 4e** show that CO_2, CH_4, and C_2H_m increased when rising $\dot{m}_{EFB}$ and their highest values were found at the maximum $\dot{m}_{EFB}$. For example, at 1300 °C, the highest CO_2, CH_4, and C_2H_m yields were 4.9, 2.8, and 0.1 mmol/$g_{dry\ biomass}$, respectively. Noticeably, CO_2, CH_4, and C_2H_m decreased while increasing the temperature thanks to the improvement of gasification reaction kinetics, in agreement with thermodynamic analysis (Chuayboon & Abanades, 2021). For instance, at 1.0 g/min, CO_2, CH_4, and C_2H_m declined from 6.9, 4.4, and 1.7 mmol/$g_{dry\ biomass}$ at 1100 °C to 4.3, 2.1, and 0.7 mmol/$g_{dry\ biomass}$ at 1300 °C, respectively. Therefore, while keeping a high $\dot{m}_{EFB}$, the amounts of CO_2, CH_4, and C_2H_m can be lowered by increasing the temperature to improve both syngas quality and syngas yield.

As shown in **Fig. 4f**, there was a significant rise in the total syngas yield with increasing $\dot{m}_{EFB}$, and the highest total syngas yield was found to be 81.1 mmol/$g_{dry\ biomass}$ at 1300 °C (which closely approached the theoretical syngas yield of 85.2 mmol/$g_{dry\ biomass}$, calculated from **Eq. 1**), followed by 71.6 mmol/$g_{dry\ biomass}$ at 1200 °C, and 61 mmol/$g_{dry\ biomass}$ at 1100 °C.

During on-sun EFB gasification, there was an issue associated with the pyrolytic smoke formation, especially when $\dot{m}_{EFB}$ was extremely high. This concern was thus experimentally investigated by determining the carbon consumption rate as a function of $\dot{m}_{EFB}$ at 1100-1300 °C. Note that the carbon consumption rate (representing the overall gasification rate) was calculated from the summation of carbon contained in the CO, CO_2, and CH_4 production rates. The carbon consumption rate as a function of $\dot{m}_{EFB}$ is plotted at 1100 °C, 1200 °C, and 1300 °C, and compared with the ideal carbon consumption rate (equal to the feeding rate), according to **Fig. 5**.

As a result, at any $\dot{m}_{EFB}$, the carbon consumption rate increased with increasing temperature, highlighting an enhanced gasification rate promoted by the temperature effect. For example, at 1300 °C, the carbon consumption rate was typically equal to the ideal value, especially at 0.6 and 1.0 g/min, demonstrating that the reactant feeding rate was equal to the rate of gasification reaction (thus denoting an absence of kinetic limitation). When increasing $\dot{m}_{EFB}$ further, the carbon consumption rate fell below the ideal line. This pointed out that the gasification rate was lower than EFB biomass feeding rate. In this case, when the carbon consumption rate was significantly lower than the ideal line, carbon accumulation in the reactor (due to incomplete biomass gasification) may occur, which then led to pyrolytic smoke. This issue most favorably occurred at the temperature of 1100 °C due to slow kinetics.

At any specified temperature, the rate of carbon consumption rose, reached a peak, and subsequently decreased with increasing $\dot{m}_{EFB}$, in agreement with the syngas yield trend, thus indicating the existence of an optimal value of $\dot{m}_{EFB}$. As the temperature increased, the maximum carbon consumption rate shifted to a higher value of $\dot{m}_{EFB}$, proving that the optimal $\dot{m}_{EFB}$ point depends on temperature, and it can be increased by rising the temperature.

In summary, the effect of $\dot{m}_{EFB}$ was highlighted as it played a key role in the continuous solar gasification of EFB. Regardless of the temperature, an increase in $\dot{m}_{EFB}$ promoted the syngas yield despite favoring untargeted CO_2, CH_4 and C_2H_m. However, an excessively high $\dot{m}_{EFB}$ downgraded syngas yield and quality. Thus, the optimal point of $\dot{m}_{EFB}$ at each operating gasification temperature is highly important in order to maximize syngas yield and gasification performance, and its value can be increased by increasing the temperature.

3.4 Solar reactor performances and efficiencies

The evolutions of the solar reactor performance and efficiencies with $\dot{m}_{EFB}$ are plotted in **Fig. 6**, consisting of solar thermal power input ($\dot{Q}_{solar}$, **Fig. 6a**), solid carbon conversion (X_C, **Fig. 6b**), energy upgrade factor (U, **Fig. 6c**), and solar-to-fuel energy conversion efficiency ($\eta_{solar\text{-}to\text{-}fuel}$, **Fig. 6d**) at 1100, 1200, and 1300 °C. As a result, $\dot{Q}_{solar}$ increased with $\dot{m}_{EFB}$, and it significantly rose with temperature (**Fig. 6a**). $\dot{Q}_{solar}$ was found in the range 1.1-1.3 kW at 1300 °C, 0.9-1.1 kW at 1200 °C, and 0.8-0.9 kW at 1100 °C. This can be explained by the fact that increasing $\dot{m}_{EFB}$ required a higher $\dot{Q}_{solar}$ to drive the endothermal gasification reaction. Similarly, $\dot{Q}_{solar}$ increased consistently when increasing the temperature. Thus, the solar energy consumption rate was increased when increasing either $\dot{m}_{EFB}$ or temperature.

At any temperature, X_C increased, reached a peak, and decreased with increasing $\dot{m}_{EFB}$, which is consistent with the trends of both the CO yield (**Fig. 4b**) and carbon consumption rate (**Fig. 5**), thereby confirming the existence of the optimal $\dot{m}_{EFB}$ at each temperature. The highest X_C value was up to 96.9% at 1300 °C, indicating that solid EFB was almost completely converted to syngas. X_C decreased slightly to 89.6% at 1200 °C and to 86.4% at 1100 °C. U exceeded one for all the tested conditions, demonstrating that the calorific value of products was higher than that of reactants thanks to solar energy storage into syngas. It reached a maximum value as high as 1.38 at 1300 °C, indicating that the energy content of products was almost 40% higher than that of reactants. Importantly, the maximum U value of 1.38 at 1300 °C approached the ideal U value of 1.39 (calculated based on **Eq. 1**), thus pointing out noteworthy performance of the continuous solar gasification process. U decreased reasonably when lowering the temperature to 1200 °C (1.14-1.23) and 1100 °C (1.10-1.16). In addition, the evolutions of U were similar to the X_C curves, thus confirming the optimal $\dot{m}_{EFB}$ at 1.8 g/min (1300 °C) and 1.0 g/min (1200 °C) where U was maximized. Except for the experiment at 1100 °C, the U curves increased linearly with $\dot{m}_{EFB}$ due to an increase in C_2H_m (**Fig. 4e**). In spite of an increase in the solar power input (**Fig. 6a**),

$\eta_{solar\text{-}to\text{-}fuel}$ still increased with increasing $\dot{m}_{EFB}$ (**Fig. 6d)** thanks to both an improvement in syngas production yield and shortened duration in biomass injection period, which in turn reduced solar energy consumption. In addition, $\eta_{solar\text{-}to\text{-}fuel}$ evolution trends were similar to both U and X_C, especially at 1300 °C, which definitely confirm the optimal $\dot{m}_{EFB}$ (1.8 g/min at 1300 °C). The maximum $\eta_{solar\text{-}to\text{-}fuel}$ approached 20% at 1300 °C, and then decreased to 17% at 1200 °C and to 14% at 1100 °C, respectively.

In summary, an increase in $\dot{m}_{EFB}$ and temperature drastically enhanced the reactor performances including X_C, U, as well as $\eta_{solar\text{-}to\text{-}fuel}$, at the expense of increased solar power input. The optimal point of $\dot{m}_{EFB}$ at any specified temperature can also be reflected by reactor performances such as X_C, U, and $\eta_{solar\text{-}to\text{-}fuel}$ curves, which are consistent with syngas yields (CO and H_2) trends. The existence and identification of an optimal point of $\dot{m}_{EFB}$ was highly beneficial for maximizing syngas production capacity and reactor performance in continuous solar EFB gasification. These results can thus be used to guideline in up-scaling the EFB gasification system. Several key outcomes of the study can further be underlined:

(i) On-sun continuous steam gasification of biowaste agricultural EFB biomass was successfully performed under real solar irradiation conditions.

(ii) Stable continuous EFB gasification was demonstrated with a steady syngas production rate over time.

(iii) EFB biomass-to-syngas conversion was accomplished with carbon conversion approaching 97%.

(iv) High global mass balance exceeding 96% confirmed reliable system.

(v) A rise in the EFB biomass feeding rate improved gasification reaction, biomass consumption, syngas production rate, and syngas yield.

(vi) An increase in the temperature enabled to expand the EFB biomass feeding rate limit, which can enhance the syngas production capacity.

(vii) An optimum in the EFB biomass feeding rate regarding maximum syngas yield and reactor performance was found to be 1.4 g/min at 1300 °C and 1.0 g/min at 1200 °C.

(viii) The highest energy upgrade factor up to 1.38 was achieved, which closely approached the ideal U value of 1.39, reflecting very high EFB-to-syngas conversion efficiency and substantially outperforming the conventional auto-thermal gasification process.

(ix) The solar-to-fuel energy conversion efficiency approached 20%, revealing efficient solar energy storage into syngas.

(x) Agricultural biowaste EFB resource was proved to be compatible with continuous solar gasification for ultimate conversion to clean and dispatchable synthetic fuel.

4. Conclusions

A biological solid waste from oil palm empty fruit bunch (EFB) in Thailand was used to experimentally investigate continuous solar-driven steam gasification for producing carbon-neutral and high-quality syngas in a solar chemical reactor. The process was conducted under real solar irradiation conditions to demonstrate the reliability and robustness of the system, which was beneficial for a scalable process. Syngas was successfully produced from the combination of two renewable resources regarding agricultural EFB biowaste and solar energy in a single process, thus offering a promising solution for converting them to clean and dispatchable chemical fuels. On-sun continuous solar gasification of EFB was carried out under different EFB biomass feeding rates (0.8-1.8 g/min) at specified gasification temperatures (1100-1300 °C). The impact of both temperature and EFB biomass feeding rate on syngas yield and solar reactor performance was addressed, and an optimal EFB biomass feeding rate at each considered temperature was highlighted. Noticeably, the EFB feeding rate exhibited a key role in continuous solar gasification performances regarding syngas production rate, yield, and energy conversion efficiency, and the optimal EFB feeding rate was experimentally identified for performance optimization. A relationship between EFB feeding rate and carbon consumption rate was also evidenced in the temperature range 1100-1300 ºC. The dynamic control of the waste feeding rate is necessary to ensure continuous solar gasifier operation under variable or intermittent solar conditions. Solar-to-fuel energy conversion efficiency can be further improved by solar reactor scaling-up, to reduce heat losses while enhancing syngas production capacity. Hybrid solar auto-thermal gasification is recommended for this system to support the fluctuating solar irradiation conditions in Thailand and operate the system around-the-clock. Solar thermochemical gasification promotes waste and biomass valorization and offers an efficient means of storing intermittent solar energy into renewable fuels. Agricultural biowaste from oil palm resource was proved to be compatible with continuous solar gasification for ultimate conversion and valorization to carbon-neutral synthetic fuels. Such a solar process could also be applied to convert other agricultural or crop residues, and the effect of the waste type and composition should be investigated. Techno-economic analysis of the solar-driven waste valorization process is recommended to further demonstrate its feasibility and viability for industrial application.

Acknowledgements

This work was supported by King Mongkut's Institute of Technology Ladkrabang [grant number: KREF046404] and French Embassy in Thailand under the Junior research fellowship program 2021.

References

Abanades, S., Rodat, S., Boujjat, H. 2021. Solar Thermochemical Green Fuels Production: A Review of Biomass Pyro-Gasification, Solar Reactor Concepts and Modelling Methods. *Energies*, **14**(5), 1494.

Al-Muraisy, S.A.A., Soares, L.A., Chuayboon, S., Ismail, S.B., Abanades, S., van Lier, J.B., Lindeboom, R.E.F. 2022. Solar-driven steam gasification of oil palm empty fruit bunch to produce syngas: Parametric optimization via central composite design. *Fuel Process. Technol.*, **227**, 107118.

Ashokkumar, V., Venkatkarthick, R., Jayashree, S., Chuetor, S., Dharmaraj, S., Kumar, G., Chen, W.-H., Ngamcharussrivichai, C. 2022. Recent advances in lignocellulosic biomass for biofuels and value-added bioproducts - A critical review. *Bioresour. Technol.*, **344**, 126195.

Basha, M.H., Sulaiman, S.A., Uemura, Y. 2020. Co-gasification of palm kernel shell and polystyrene plastic: Effect of different operating conditions. *J. Energy Inst.*, **93**(3), 1045-1052.

Beck, F., Martinot, E. 2004. Renewable Energy Policies and Barriers. in: *Encyclopedia of Energy*, (Ed.) C.J. Cleveland, Elsevier. New York, pp. 365-383.

Bellouard, Q., Abanades, S., Rodat, S., Dupassieux, N. 2017. Solar thermochemical gasification of wood biomass for syngas production in a high-temperature continuously-fed tubular reactor. *Int. J. Hydrogen Energy*, **42**(19), 13486-13497.

Bonechi, C., Consumi, M., Donati, A., Leone, G., Magnani, A., Tamasi, G., Rossi, C. 2017. 1 - Biomass: An overview. in: *Bioenergy Systems for the Future*, (Eds.) F. Dalena, A. Basile, C. Rossi, Woodhead Publishing, pp. 3-42.

Boujjat, H., Rodat, S., Abanades, S. 2020a. Solar-hybrid Thermochemical Gasification of Wood Particles and Solid Recovered Fuel in a Continuously-Fed Prototype Reactor. *Energies*, **13**(19), 5217.

Boujjat, H., Rodat, S., Abanades, S. 2021. Techno-Economic Assessment of Solar-Driven Steam Gasification of Biomass for Large-Scale Hydrogen Production. *Processes*, **9**(3), 462.

Boujjat, H., Rodat, S., Chuayboon, S., Abanades, S. 2020b. Experimental and CFD investigation of inert bed materials effects in a high-temperature conical cavity-type reactor for continuous solar-driven steam gasification of biomass. *Chem. Eng. Sci.*, **228**, 115970.

Boujjat, H., Rodat, S., Chuayboon, S., Abanades, S. 2019a. Experimental and numerical study of a directly irradiated hybrid solar/combustion spouted bed reactor for continuous steam gasification of biomass. *Energy*, **189**, 116118.

Boujjat, H., Rodat, S., Chuayboon, S., Abanades, S. 2019b. Numerical simulation of reactive gas-particle flow in a solar jet spouted bed reactor for continuous biomass gasification. *Int. J. Heat Mass Transfer*, **144**, 118572.

Boujjat, H., Yuki Junior, G.M., Rodat, S., Abanades, S. 2020c. Dynamic simulation and control of solar biomass gasification for hydrogen-rich syngas production during allothermal and hybrid solar/autothermal operation. *Int. J. Hydrogen Energy*, **45**(48), 25827-25837.

Chimres, N., Wongwises, S. 2016. Critical review of the current status of solar energy in Thailand. *Renew. Sust. Energ. Rev.*, **58**, 198-207.

Chu, P., Hu, Q., Chen, J., Loh, C.Y.-A., Lin, A., Li, X., Chen, D., Leong, K., Dai, Y., Wang, C.-H. 2022. Performance analysis of a pilot-scale municipal solid waste gasification and dehumidification system for the production of energy and resource. *Energy Convers. Manage.*, **258**, 115505.

Chuayboon, S., Abanades, S. 2020. An overview of solar decarbonization processes, reacting oxide materials, and thermochemical reactors for hydrogen and syngas production. *Int. J. Hydrogen Energy*, **45**(48), 25783-25810.

Chuayboon, S., Abanades, S. 2021. Thermodynamic and Experimental Investigation of Solar-Driven Biomass Pyro-Gasification Using H2O, CO2, or ZnO Oxidants for Clean Syngas and Metallurgical Zn Production. *Processes*, **9**(4), 687.

Chuayboon, S., Abanades, S., Rodat, S. 2018a. Comprehensive performance assessment of a continuous solar-driven biomass gasifier. *Fuel Process. Technol.*, **182**, 1-14.

Chuayboon, S., Abanades, S., Rodat, S. 2018b. Experimental analysis of continuous steam gasification of wood biomass for syngas production in a high-temperature particle-fed solar reactor. *Chem. Eng. Process.*, **125**, 253-265.

Chuayboon, S., Abanades, S., Rodat, S. 2019. Insights into the influence of biomass feedstock type, particle size and feeding rate on thermochemical performances of a continuous solar gasification reactor. *Renew. Energy*, **130**, 360-370.

Chuayboon, S., Abanades, S., Rodat, S. 2018c. Solar chemical looping gasification of biomass with the ZnO/Zn redox system for syngas and zinc production in a continuously-fed solar reactor. *Fuel*, **215**, 66-79.

Dechapanya, W., Rattanahirun, S., Khamwichit, A. 2020. Syngas Production From Palm Kernel Shells With Enhanced Tar Removal Using Biochar From Agricultural Residues†. *Front. Energy Res.*, **8**.

Hossain, M.A., Jewaratnam, J., Ganesan, P. 2016. Prospect of hydrogen production from oil palm biomass by thermochemical process – A review. *Int. J. Hydrogen Energy*, **41**(38), 16637-16655.

Jahromi, R., Rezaei, M., Hashem Samadi, S., Jahromi, H. 2021. Biomass gasification in a downdraft fixed-bed gasifier: Optimization of operating conditions. *Chem. Eng. Sci.*, **231**, 116249.

Kabli, M.R., Ali, A.M., Inayat, M., Zahrani, A.A., Shahzad, K., Shahbaz, M., Sulaiman, S.A. 2022. H2-rich syngas production from air gasification of date palm waste: an experimental and modeling investigation. *Biomass Conv. Bioref.*

Lapuerta, M., Hernández, J.J., Pazo, A., López, J. 2008. Gasification and co-gasification of biomass wastes: Effect of the biomass origin and the gasifier operating conditions. *Fuel Process. Technol.*, **89**(9), 828-837.

Li, J., Yin, Y., Zhang, X., Liu, J., Yan, R. 2009. Hydrogen-rich gas production by steam gasification of palm oil wastes over supported tri-metallic catalyst. *Int. J. Hydrogen Energy*, **34**(22), 9108-9115.

Lichty, P., Perkins, C., Woodruff, B., Bingham, C., Weimer, A. 2010. Rapid High Temperature Solar Thermal Biomass Gasification in a Prototype Cavity Reactor. *J. Sol. Energy Eng.*, **132**(1).

Ling, J.L.J., Go, E.S., Park, Y.-K., Lee, S.H. 2022. Recent advances of hybrid solar-Biomass thermo-chemical conversion systems. *Chemosphere*, **290**, 133245.

Materazzi, M., Taylor, R. 2019. 18 - The GoGreenGas case in the UK. in: *Substitute Natural Gas from Waste*, (Eds.) M. Materazzi, P.U. Foscolo, Academic Press, pp. 475-495.

Mohammed, M.A.A., Salmiaton, A., Wan Azlina, W.A.K.G., Mohamad Amran, M.S. 2012. Gasification of oil palm empty fruit bunches: A characterization and kinetic study. *Bioresour. Technol.*, **110**, 628-636.

Moriarty, P., Honnery, D. 2019. 6 - Global renewable energy resources and use in 2050. in: *Managing Global Warming*, (Ed.) T.M. Letcher, Academic Press, pp. 221-235.

Nipattummakul, N., Ahmed, I.I., Gupta, A.K., Kerdsuwan, S. 2011. Hydrogen and syngas yield from residual branches of oil palm tree using steam gasification. *Int. J. Hydrogen Energy*, **36**(6), 3835-3843.

Omar, R., Idris, A., Yunus, R., Khalid, K., Aida Isma, M.I. 2011. Characterization of empty fruit bunch for microwave-assisted pyrolysis. *Fuel*, **90**(4), 1536-1544.

Pohjakallio, M., Vuorinen, T., Oasmaa, A. 2020. Chapter 13 - Chemical routes for recycling—dissolving, catalytic, and thermochemical technologies. in: *Plastic Waste and Recycling*, (Ed.) T.M. Letcher, Academic Press, pp. 359-384.

Prasertsan, S., Prasertsan, P. 1996. Biomass residues from palm oil mills in Thailand: An overview on quantity and potential usage. *Biomass Bioenergy*, **11**(5), 387-395.

Prasertsan, S., Sajjakulnukit, B. 2006. Biomass and biogas energy in Thailand: Potential, opportunity and barriers. *Renew. Energy*, **31**(5), 599-610.

Rodat, S., Abanades, S., Boujjat, H., Chuayboon, S. 2020. On the path toward day and night continuous solar high temperature thermochemical processes: A review. *Renew. Sust. Energ. Rev.*, **132**, 110061.

Roshan Kumar, T., Mattisson, T., Rydén, M., Stenberg, V. 2022. Process Analysis of Chemical Looping Gasification of Biomass for Fischer–Tropsch Crude Production with Net-Negative CO2 Emissions: Part 1. *Energy Fuels*, **36**(17), 9687-9705.

Sarasuk, K., Sajjakulnukit, B. 2011. Design of a Lab-Scale Two-Stage Rice Husk Gasifier. *Energy Procedia*, **9**, 178-185.

Shuit, S.H., Tan, K.T., Lee, K.T., Kamaruddin, A.H. 2009. Oil palm biomass as a sustainable energy source: A Malaysian case study. *Energy*, **34**(9), 1225-1235.

Steven, S., Restiawaty, E., Bindar, Y. 2021. Routes for energy and bio-silica production from rice husk: A comprehensive review and emerging prospect. *Renew. Sust. Energ. Rev.*, **149**, 111329.

Sun, Z., Aziz, M. 2022. Solar-assisted biomass chemical looping gasification in an indirect coupling: Principle and application. *Applied Energy*, **323**, 119635.

Thomas, J.M.G., Prasad, P.V.V. 2003. PLANTS AND THE ENVIRONMENT | Global Warming Effects. in: *Encyclopedia of Applied Plant Sciences*, (Ed.) B. Thomas, Elsevier. Oxford, pp. 786-794.

Tsai, W.-T. 2019. Benefit Analysis and Regulatory Actions for Imported Palm Kernel Shell as an Environment-Friendly Energy Source in Taiwan. *Resources*, **8**(1), 8.

Vargas-Mira, A., Zuluaga-García, C., González-Delgado, Á.D. 2019. A Technical and Environmental Evaluation of Six Routes for Industrial Hydrogen Production from Empty Palm Fruit Bunches. *ACS Omega*, **4**(13), 15457-15470.

Yang, H., Yan, R., Chen, H., Lee, D.H., Liang, D.T., Zheng, C. 2006. Pyrolysis of palm oil wastes for enhanced production of hydrogen rich gases. *Fuel Process. Technol.*, **87**(10), 935-942.

You, S., Ok, Y.S., Chen, S.S., Tsang, D.C.W., Kwon, E.E., Lee, J., Wang, C.-H. 2017. A critical review on sustainable biochar system through gasification: Energy and environmental applications. *Bioresour. Technol.*, **246**, 242-253.

Table 1. Characteristics, ultimate and proximate analysis of the EFB from oil palm.

Biomass	LHV (MJ/kg)	Bulk density (g/cm^3)	Particle size (mm)	Proximate analysis (wt % dry basis)			Ultimate analysis (wt % dry basis)					
				Volatile matter	Fixed carbon	Moisture	C	H	O	S	N	Ash
EFB	16.2	0.17± 0.02	1-2	79.2±1.2	17.1±1.1	9.3±0.5	49.6±0.5	7.1±0.1	46.1±0.4	0.05±0.1	0.5±0.1	1.3±0.01

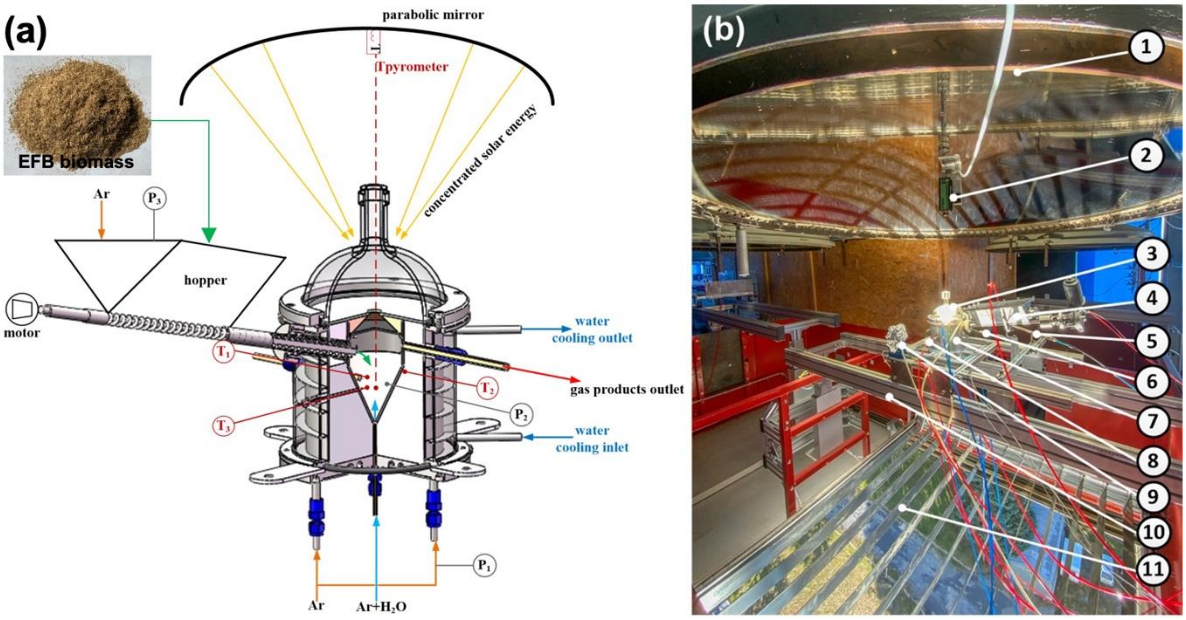

Fig. 1. (a) Schematic diagram of the solar reactor and (b) photograph of on-sun continuous steam gasification of EFB: (1) parabolic dish concentrator, (2) pyrometer, (3) transparent window, (4) biomass feeding system, (5) syngas outlet port, (6) thermocouple type B (T_1), (7) water-cooled reactor shell, (8) pressure transducer, (9) H_2O mass flow controller, (10) reactor frame which can be moved in upward or downward directions for focal point adjustment at the cavity aperture, (11) automatic shutter to control solar power input.

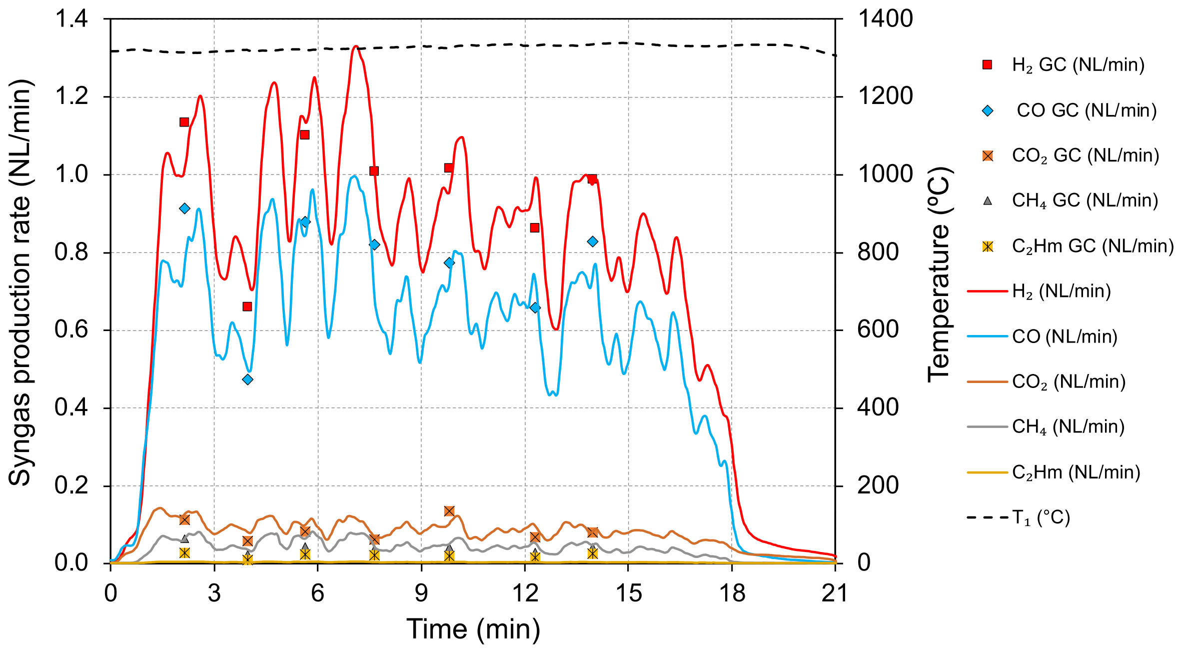

Fig. 2. Representative experimental run of continuous solar-driven steam gasification of EFB. Experimental conditions: T_1 = 1300 °C, EFB feeding rate = 1.0 g/min and steam/EFB molar ratio = 2.2.

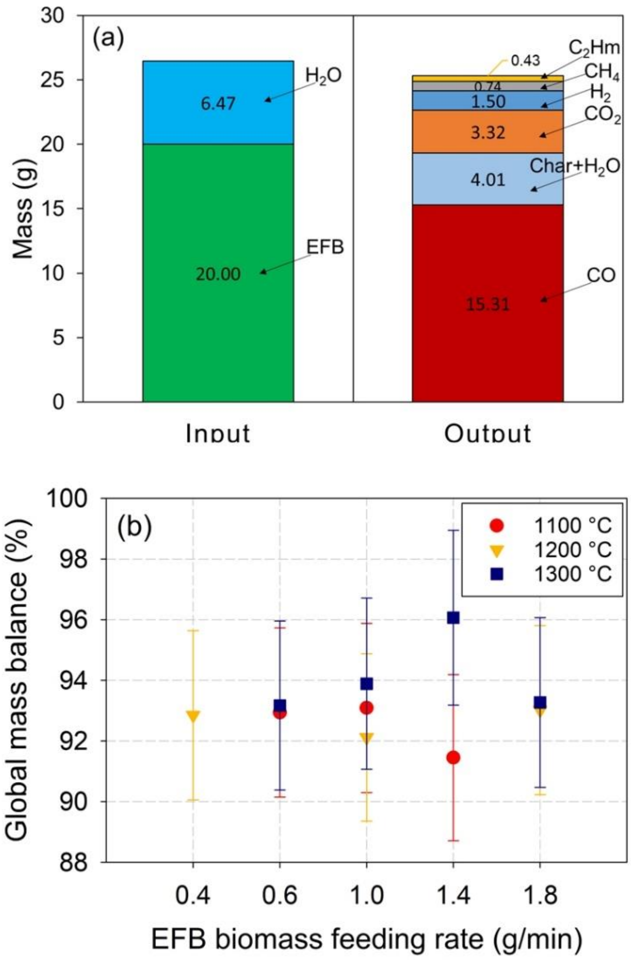

Fig. 3. (a) Comparison of experimental mass measurements between input reactants and output products, and (b) global mass balance as a function of biomass feeding rate at temperatures of 1100, 1200, and 1300 °C.

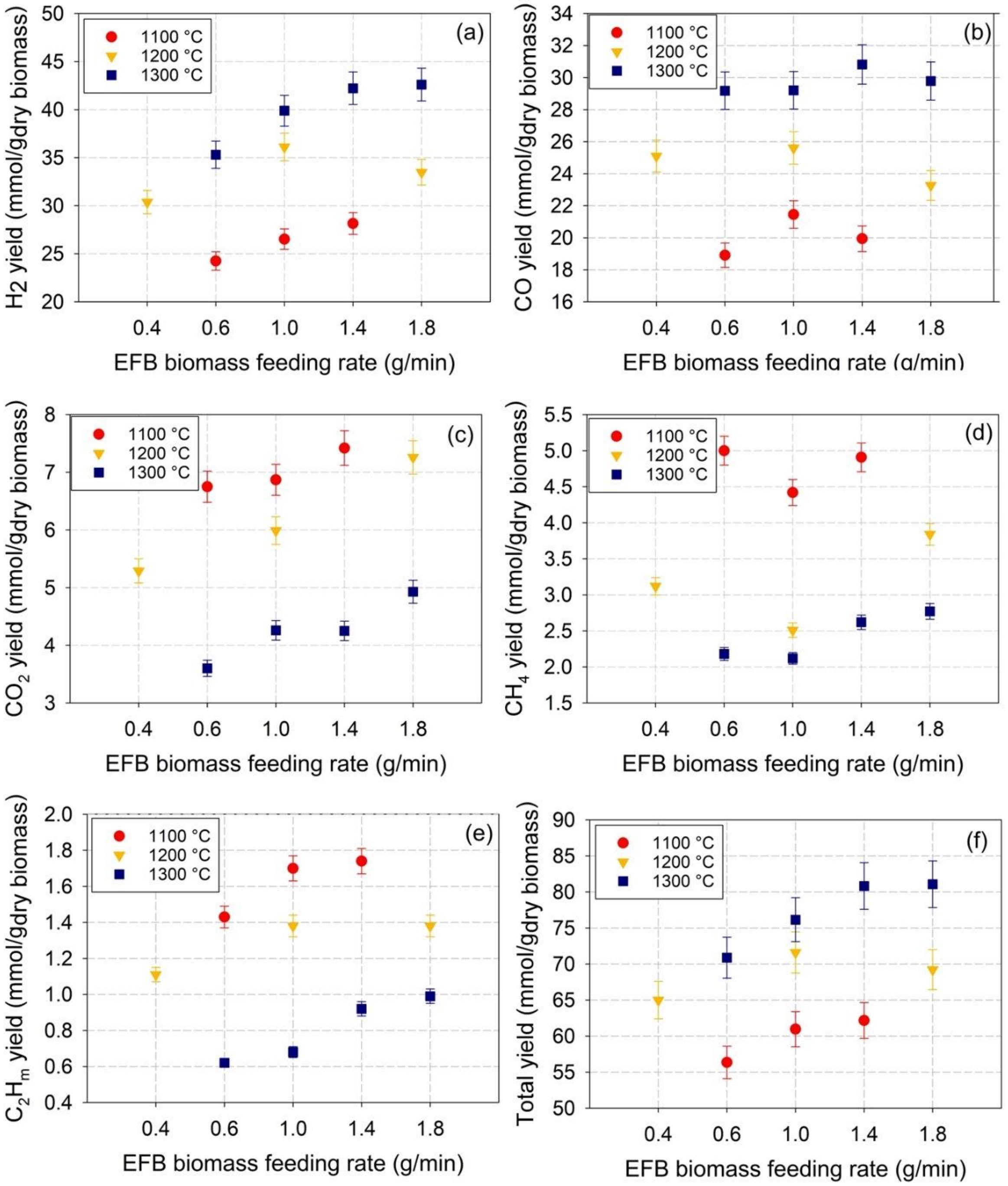

Fig. 4. Syngas yields as a function of EFB biomass feeding rate at 1100, 1200, and 1300 °C: (a) H_2, (b) CO, (c) CO_2, (d) CH_4, (e) C_2H_m, and (f) total syngas yield.

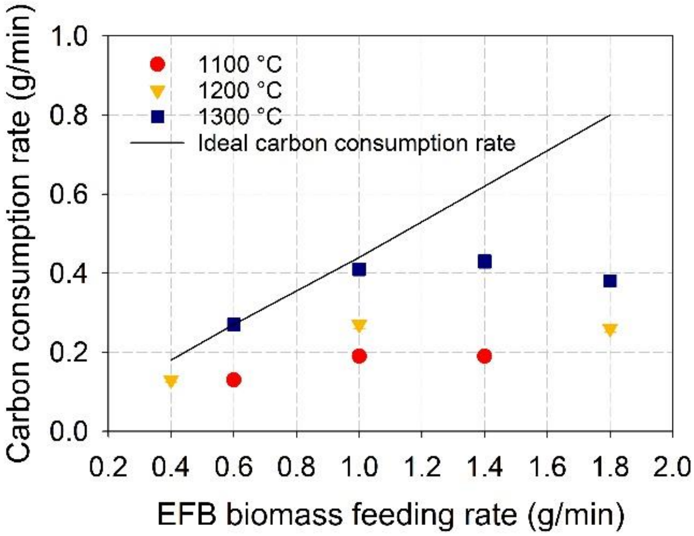

Fig. 5. Carbon consumption rate as a function of EFB biomass feeding rate at 1100-1300 °C.

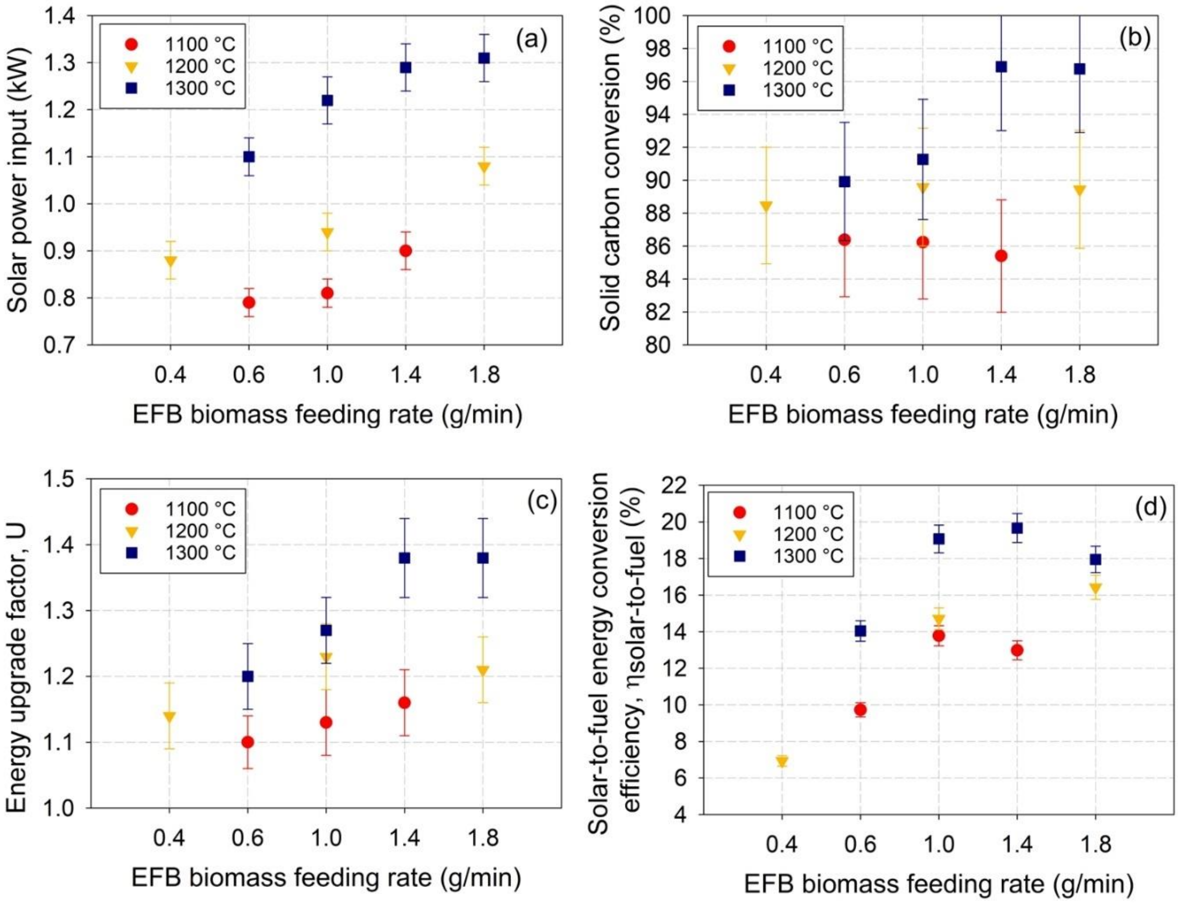

Fig. 6. Solar power input, solid carbon conversion, energy upgrade factor, and solar-to-fuel energy conversion efficiency versus EFB feeding rate at different temperatures.